

Nanoscale Advances

Accepted Manuscript

This article can be cited before page numbers have been issued, to do this please use: B. Favelukis, B. Ratzker, R. Miyar, J. Jopp, A. Upcher, P. Shekhter, N. maman and M. Sokol, *Nanoscale Adv.*, 2025, DOI: 10.1039/D4NA00983E.



This is an Accepted Manuscript, which has been through the Royal Society of Chemistry peer review process and has been accepted for publication.

Accepted Manuscripts are published online shortly after acceptance, before technical editing, formatting and proof reading. Using this free service, authors can make their results available to the community, in citable form, before we publish the edited article. We will replace this Accepted Manuscript with the edited and formatted Advance Article as soon as it is available.

You can find more information about Accepted Manuscripts in the [Information for Authors](#).

Please note that technical editing may introduce minor changes to the text and/or graphics, which may alter content. The journal's standard [Terms & Conditions](#) and the [Ethical guidelines](#) still apply. In no event shall the Royal Society of Chemistry be held responsible for any errors or omissions in this Accepted Manuscript or any consequences arising from the use of any information it contains.

Without a Grain of Salt: Micropatterning Clean MXene Thin-Film Electronics

View Article Online
DOI: 10.1039/D4NA00983E

Bar Favelukis¹, Barak Ratzker¹, Rebeca Miyar¹, Jürgen Jopp², Alexander Upcher², Pini Shekhter³, Nitzan Maman², Maxim Sokol^{1,*}

¹ Department of Materials Science and Engineering, Tel Aviv University, P.O.B 39040, Ramat Aviv 6997801, Israel

² Ilse Katz Institute for Nanoscale Science and Technology, Ben-Gurion University of the Negev, P.O.B 653 Beer-Sheva 8410501, Israel

³ Tel Aviv University Center for Nanoscience and Nanotechnology, Tel Aviv University, P.O.B 39040, Ramat Aviv 6997801, Israel

Abstract

MXenes exhibits remarkable electrical, mechanical, and thermal properties, positioning them as strong candidates for high-performance electrodes and interconnects. Deposited 2D MXene thin-films suffer from a persistent issue of crystalline salt residues that originate from dissolved intercalation salts used for the exfoliation process during synthesis. These 3D salt residues can cause issues during further nanofabrication processing and be detrimental to integrated device performance. This study introduces a 3-step approach involving spin-coating deposition, HCl spin-cleaning, and lift-off. Rigorous morphological characterization of the patterned MXene was performed, confirming that the spin-cleaning step effectively removed all halide salt residues. Transparent sub-10 nm-thick MXene thin-film electrodes, down to a width of 5 μm with $\sim 1.5 \mu\text{m}$ resolution, were produced. The electrical properties were probed, showcasing exceptional conductivity ($\sim 1350 \text{ S/cm}$ for a 50 μm -wide electrode), with high photosensitivity at the MXene–Si junction. The proposed method yields clean patterned MXene thin films, enabling easier integration of MXene or other 2D materials into future microelectronic devices.

Keywords: $\text{Ti}_3\text{C}_2\text{T}_z$ MXene; HCl; spin-coating; lithography; microelectronics

1. Introduction

Technological advancements and device miniaturization in microelectronics continuously push the limits of current materials capabilities¹. As integrated circuits become more powerful or feature smaller components, conventional metal interconnects face significant challenges, including high resistivity, electromigration, and reliability issues². The need to replace traditional metal electrodes and interconnects is driven further by the demand for transparent, flexible, and wearable electronics. A promising solution is the thin-film deposition of 2D inorganic materials for next-generation electronics³. Currently, most low-dimensional electrode materials face significant challenges related to high synthesis temperatures and limitations in scalable manufacturing^{4–7}.



MXenes, an emerging diverse family of 2D transition metal carbides/nitrides, are a promising alternative to overcome said challenges^{8–10}. The synthesis of MXene involves selectively etching the "A" element out of the MAX phases to form the general formula $M_{n+1}X_nT_z$ ($n=1-4$), where "M" is an early transition metal, "X" represents carbon or nitrogen, and "T_z" represents surface terminations, usually -O, -OH, or -F¹¹. Colloidal solutions of single-layer MXene are prepared by exfoliation of multilayer MXene intercalated with halide or organic salts (e.g., LiF, LiCl, TMAOH, etc.) during or after etching¹¹.

Unlike other 2D materials, MXene can be synthesized in large batches and directly exfoliated into a colloidal solution, simplifying processing scalability and avoiding complex surface modification requirements^{12,13}. MXenes are known for their high electrical conductivity and have been shown to withstand high breakdown current densities ($\sim 1.2 \cdot 10^8 \text{ Acm}^{-2}$)². Another advantage is the tunability of their work function, for example $Ti_3C_2T_z$ can exhibit a work function ranging from 3.9 to 4.8 eV, depending on surface terminations^{14,15}. Precisely controlling the thickness of the deposited MXene thin films (<20 nm) enables fabrication of transparent microelectronic components with high conductivity^{16,17}. To realize MXene-based microelectronics a variety of deposition methods can be employed¹⁸. MXene deposition can be performed using spray coating¹⁹, dip coating²⁰, blade coating²¹, inkjet printing²², and spin coating^{22,23}. Followed by patterning techniques such as reactive ion etching²⁴, deposition over a photoresist and subsequent lift-off^{25–27}, and microscale contact printing²⁸.

The deposition of MXene films requires using MXene colloids that contain unavoidable traces of dissolved halide salts (used for intercalation)¹¹. Therefore, once the MXene colloid dries up, salt residues always crystallize on the MXene films^{16,18,26,29–31}. This issue is currently overlooked as the salt residues sit on top of the film and have a negligible effect on the performance of the MXene itself. However, the presence of salt residues will present challenges for future integration of MXenes with other materials in more complex integrated 2D microelectronic systems. The salt crystals 3D structure obstructs 2D layered construction and their high volatility can be extremely detrimental during nanofabrication processes at elevated temperatures³¹. In addition, alkali metal (e.g., Li) and other contaminations (e.g., F) can alter desired electronic properties and even lead to catastrophic failure of the electronic device³¹. Therefore, integrating a step to eliminate salt residues during the fabrication process is imperative.

Previous studies have demonstrated deposition and patterning of MXene films^{24,25,27,28,32–34}, however almost none have addressed the issue of salt residues³⁵. In addition, lift-off related morphological defects, nor the electrical properties of microscale features have only been superficially addressed¹⁸. Herein we demonstrate an effective spin-coating fabrication process for MXenes that involves a subsequent salt removal step by spin cleaning using HCl. The microstructure of the obtained MXene micropatterned features were characterized in-depth and the microscale electronic properties were assessed.

2. Experimental section

2.1 Materials synthesis

2.1.1 MAX phase

Ti_3AlC_2 powder was synthesized through a liquid-phase reaction. Titanium carbide (TiC 99.5%, Alfa Aesar), titanium (Ti 99.7%, Strem), aluminum (Al 99.7%, Strem) powders were



mixed in a ratio of 2:1:1.1 and tumbled in a 50 ml centrifuge tube with stainless steel balls at 200 rpm for 18 h. The mixed powders were then cold pressed in a 200 mm die at 1.5 tons, and the resulting pellet was placed in an alumina crucible. The pellet underwent heat treatment in a tube furnace at 1500 °C for 3 h, with a heating rate of 5 °C/min, under an Ar pressure of 200 sccm. Following the heat treatment, the pellet was ball-milled at 1800 rpm for 5 min and subsequently ground and sieved resulting in a ≥ 300 -mesh powder.

2.2.1 MXene

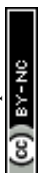
Ti₃C₂T_z MXene was synthesized by selectively etching the Al layer from the Ti₃AlC₂ MAX phase precursor. The acid solution was prepared by dissolving 1.6 g of lithium fluoride (LiF 99%, Strem) in 20 ml of Hydrochloric acid 10.2 M (HCl 32%, Bio-Lab) in a high-density polyethylene vial with a magnetic stirrer. Then, 1 g of MAX powder was slowly added to the solution. The etching process was carried out while being held at 45°C in an oil bath for 24 h. After the etching process, the mixture was centrifuged at 3500 rpm, twice 0.5 M HCl followed by several times in DI water until the pH reached 6 (and the multilayer MXene became suspended). To exfoliate the MXene the suspension was then sonicated in an ultrasonic bath for 1 h while being kept at 15°C to prevent heating. After sonication the suspension was centrifuged at 3500 rpm for 30 min to separate any unexfoliated sediment. The MXene colloidal solution was bubbled with N₂ and stored at 4°C. 5 ml of the colloid was dried and weighed to determine the MXene load which was roughly 11 g/l.

2.2 MXene deposition and patterning

Various substrates were prepared for MXene coating. A sapphire wafer (c-plane sapphire EPI ready, Semiconductor Wafer Inc., SWI), microscope glass slide (1-1.2 mm, Huida Medical Instruments Co.,Ltd), and Si wafer (100 n-type p-doped 1-100 Ωcm, University wafers) were diced into 8×8 mm square substrates using a dicer (Disco DAD 3350). In addition, n-type Si wafers with developed photoresist (AZ1518 MicroChemicals) were diced into 1×1 cm squares substrates. Following dicing all the substrates were sonicated in DI water for 7 min to remove any dicing residues. Before coating, the sapphire, glass, and Si were cleaned with piranha solution 1:3 H₂O₂/H₂SO₄, respectively, (H₂SO₄ 98% SDFCL, H₂O₂ 35% ThermoFisher Scientific) and the and Si wafers with developed photoresist were cleaned with diluted piranha solution (1:3 piranha/H₂O) for 15 min, then rinsed in DI water and dried with compressed N₂. MXene solutions with loading between 0.1 and 7 g/l were prepared and spin-coated on the Si substrates at 2000 or 3000 rpm for 90 s using spin-coater (Specialty Coating Systems, INC Spincoater Model P6700). The sapphire and glass substrates were spin-coated with MXene solutions of 7 g/l at 2000 rpm for 90 s. *Residual salt removal* was done by dripping 100 μl of 0.5 M HCl on the coated substrate over the span of 5 s while it stayed on the spin coater. The HCl together with the dissolved salt residues were removed by spinning at 2000 rpm for 90 s. The photoresist lift-off was done by acetone while spinning at 2000 rpm, followed by 80 s for drying.

2.3 Characterization

X-ray diffraction (XRD) measurements were performed on the precursor MAX phase powder and vacuum-filtered free-standing films 3 to 85 2θ in 0.02° steps using a Malvern Panalytical Aeris diffractometer with CuKα radiation. X-ray photoelectron spectroscopy (XPS) measurements were performed using ESCALAB QXi (Thermo Scientific, USA). High



resolution spectra were collected with a pass energy of 20 eV. Valence and cut-off spectra were collected with a pass energy of 5 eV and a bias of -5 V to allow for better energy resolution and clear measurement of the work function. MXene coatings and patterns were observed by optical microscopy (Motic SMZ 171) and closely examined by high-resolution scanning electron microscopy (HRSEM) at 2 kV (ZEISS Gemini 300). The size distribution of residual salt particles on deposited MXene films were analyzed by image analysis using ImageJ software. Energy-dispersive spectroscopy (EDS) analysis (Bruker X-Flash 6/60) at 15 kV was performed on deposited MXene films without HCl spin-cleaning using the same HRSEM. A thin lamella containing two regions of interest (ROI) from a 15 μm -wide electrode cross-section was prepared by dual beam focused ion beam (FIB; FEI Helios G4 UC). To protect the ROI surface from the ion beam and enable uniform preparation they were covered by 500 nm thick electron deposition of platinum followed by 3 μm ion deposition of tungsten covering the whole area. The lamella was examined using a probe Cs-corrected (S-CORR) scanning transmission electron microscope (STEM) (Thermofisher Spectra 200) operating at 200 kV. Atomic force microscopy (AFM) measurements were performed using the MFP-3D-Bio system from Asylum Research/Oxford Instruments. The measurements utilized an AC160TS probe ($f_0 = 300$ kHz, $k = 26$ N/m, nom.) from Olympus, and AC mode was used with a free amplitude (A_0) set to 2.34 V (or 200 nm). The setpoint amplitude (A_s) was set to 1.423 V (or 125 nm, which is approximately 63% of A_0). The operating frequency (f) was 283.70 kHz $< f_0$. The in-line transmittance of the glass and MXene-coated glass were measured between the wavelengths of 300-1800 nm by a spectrophotometer via a 5 mm aperture (Agilent Cary 5000).

2.6 Electrical measurements

The electrical resistivity and sheet resistance of the pristine n-type Si wafer and uniform MXene coating on sapphire and glass was determined by measuring the voltage induced by applying currents between 10-100 μA and 1-10 mA by a four-point probe (Lucas Labs 302, probe distance 1.016 mm) using a 6221 Keithley current source and 2001 multimeter. The measurements were carried out in ambient conditions.

The electrical resistivity of the patterned MXene electrodes was measured using an electric probe system (Keithley 4200A I-V/C-V) with a four-point probe configuration (probe distance 0.2 mm) using the same Keithley instruments. All measurements were repeated several times at different locations. The MXene-Si Schottky junction diode I-V curve characterization was performed using the same Keithley unit with a 2-point probe configuration and 0.04 V steps. The I-V curves were measured under various white LED illumination intensities ranging between 270-4330 lx determined using a digital LED light meter (HABOTEST HT620L). The illuminance Lux values were converted to irradiance according to $1 \text{ lx} = 0.0028 \text{ W/m}^2$ based on measurements on white LED³⁶. The measurements were carried out in ambient conditions in a cleanroom. All the measurements were repeated while changing the probe placements on various electrodes for validation.

3. Results and Discussion

3.1 MXene deposition and patterning

3.1.1 Thin-film deposition



The basic characteristics of the MAX phase precursor and the synthesized MXene are shown in the Supplementary Information (SI) (Fig. S1). The control over the spin-coated MXene coverage was achieved by adjusting the MXene solution concentrations and rpm (Fig. S2 and S3). The MXene coverage improved slightly at a lower spin speed. The distribution was even across the wafer besides the considerable accumulation at the rectangular die corners (Fig. S4). The most influential factor governing coverage is the MXene solution concentration. Above a concentration of 3 g/l, the MXene films start to become continuous. Increasing concentration also results in the presence of more abundant and larger salt residues on the deposited MXene (Fig. S5). Optimal uniform thin-film formation (>99 % coverage) was achieved using a MXene solution concentration of 7 g/l, spun at 2000 rpm. These specific MXene spin-coating parameters were consistently employed for all subsequent experiments conducted in this study.

3.1.2 Removal of salt residues

Micropatterned MXene thin films using photolithography–lift-off based techniques was achieved by a simple three-step method (Fig. 1a-c), resulting in clean MXene patterns with few-micron resolution in a streamlined procedure without removing the substrate from the spin coater. After the spin coating deposition many salt residues are observed (Fig. 1d). EDS confirmed that these residue particles contain only F (Fig. S6) and are therefore assumed to be LiF. Following the HCl spin-cleaning treatment all salt residues, ranging in sizes of ~10-500 nm, were removed (Fig. 1g). Note that the bright white spots are LiF and what remains after the cleaning process are just wrinkles in the MXene. The HCl dissolves the submicron/nano salt particles and is spin dried without any residue accumulation. Since MXene cannot be exfoliated in an acidic solution³⁷ the film remains intact and unaffected after HCl application. To date, most of the studies that demonstrated fabrication of intricate microelectronic MXene thin-film components employ methods that involve low-concentration solutions such as spray coating and dip coating which are difficult to use in large scales¹⁸. The HCl spin-cleaning treatment offers high throughput and scalability by enabling MXene deposition with very high concentration colloidal solutions that are produced with less scrutiny and contain more salt impurities. This approach could be implemented for other 2D materials synthesized by intercalation and exfoliation^{3,34,38}.

3.1.3 Patterning by lift-off

MXene deposits over both the Si and photoresist in an isotropic manner. Using the diluted piranha treatment the Si becomes more hydrophilic in comparison to the photoresist, resulting in full coverage of the Si whereas the photoresist remains partially exposed (Fig. 1e,f and Figs. S7-8a,b). This allows for a simple removal of the photoresist and in turn enables a clean lift-off process. This final step of the removal of the photoresist is done directly on the spin-coater using acetone, allowing for a seamless and facile process, yielding patterned MXene electrodes (Fig. S7 and S8). Following the lift-off step, folds 1-2 μm wide can be observed at the edges of the MXene films (Fig. 1h,i). The width of the folds matches the thickness of the photoresist. Performing the lift-off step directly on the spin-coater results in a more controlled and uniform folding as compared to lift-off without spinning (Fig. S9). The resolution limits in these processes are defined by the photoresist thickness and the average size of the MXene flakes. We demonstrated this process is effective at wafer-scale, at least up to a diameter of 4" (Fig. S10).



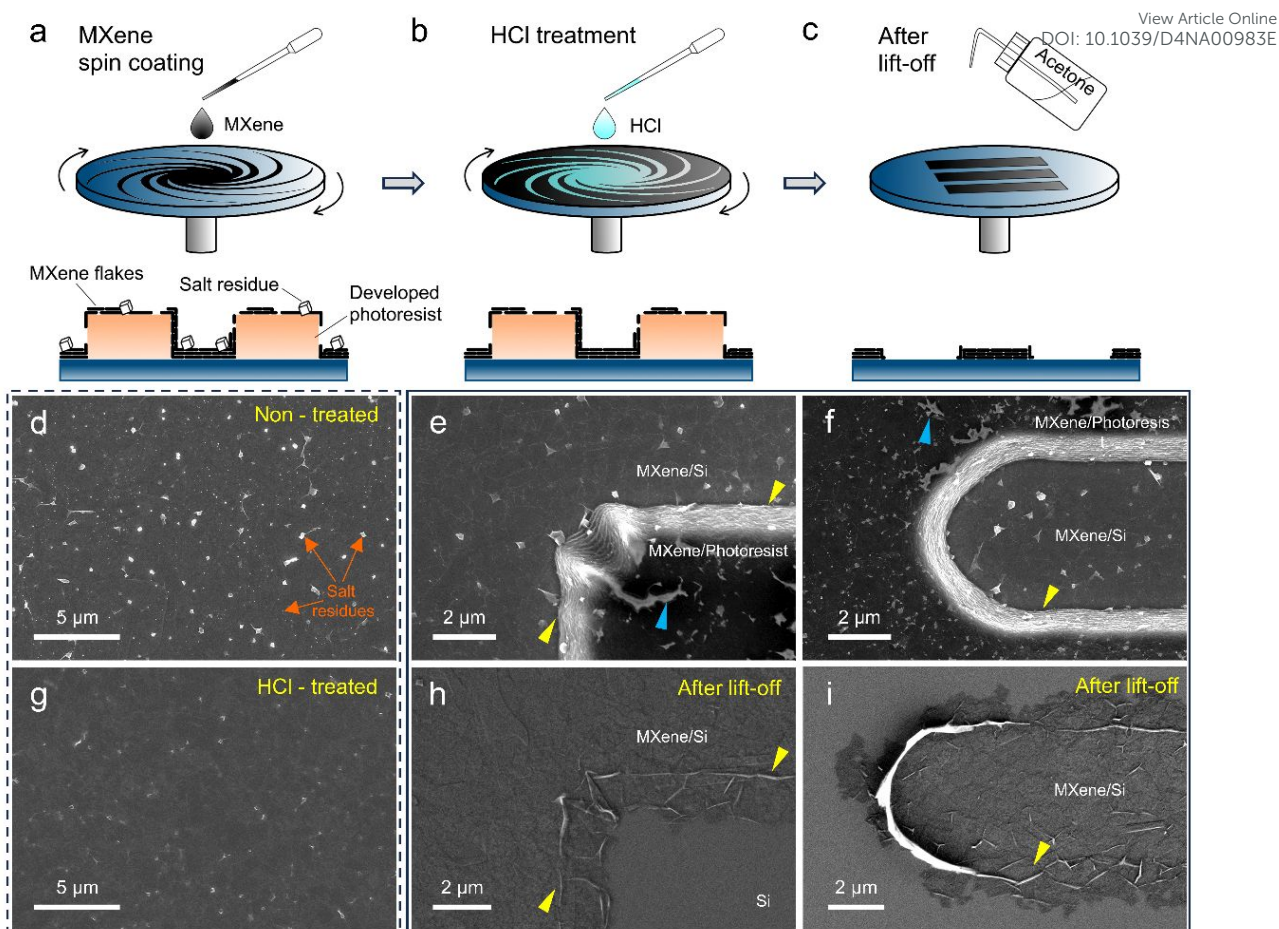


Fig. 1 Three-step process of MXene deposition, salt removal, and thin-film patterning. Schematic illustration of the process steps (a) MXene spin coating over patterned photoresist, (b) salt residue removal by HCl spin-cleaning, and (c) lift-off of the photoresist on the spin coater. SEM images of MXene thin film (d) before and (g) after HCl spin-cleaning. MXene coating on Si and developed photoresist showing a (e) corner and (f) electrode edge, exposed photoresist is indicated by blue arrowheads. MXene patterns after photoresist removal (lift-off) of similar (h) corner and (i) electrode edge. Folding and wrinkling is present at the edges where the photoresist used to be, as indicated by yellow arrowheads.

3.3 Morphological characterization of patterned MXene thin films

Lift-off of MXene thin-films creates some noticeable features in the outline of the patterns (Fig. 2a,b,c), associated with the nature of the 2D flake morphology. (1) Standing vertical films of MXene can be observed at the corner edges of patterns (Fig. 1i and 2a). (2) Distinct large wrinkles, oriented in parallel to the MXene pattern edge, persist along both sides of the patterned electrode (Fig. 2b and Fig. S9g,h). These wrinkles manifest where the edge of the photoresist used to be (Fig. 1 and Fig. S9). (3) Spill-out or inside-folding of individual flakes is intermittently observed (Fig. 2b,c). The lateral size of these defects is usually 1-1.5 μm . We suggest that optimizing the photoresist type and height will alleviate or eliminate most of these imperfections. As the formation of the edge imperfections like walls, folds, or spill-outs are sensitive to the photoresist type, thickness, and lift-off process. Ultimately, the patterning spatial resolution will be dictated by the size of the MXene flakes. Another consistent feature that is not associated with the lift-off is shallow homogenous ripples in the MXene flakes, which



can be observed at high magnifications (Fig. 2c). Despite the common occurrence of ripples in deposited MXenes, the physics behind them is still not fully understood³⁹.

The relatively large wrinkles are not typically found in MXene films formed by other means and can reach a height of up to ~60 nm (Fig. 3d), while being only ~10-20 nm wide, owing to the flexibility of MXene flakes⁴⁰. Since the large wrinkles or vertical walls exhibit a large height-to-width aspect ratio, they can perhaps be utilized to study fundamental nanoscale effects for development of optoelectronics, biosensors, energy storage, and more⁴¹.

The MXene thin film is formed by tiling and intersections of MXene flakes. The intersections between adjacent MXene flakes form line defects that resemble edge dislocations (Fig. 3f). These defects act as “grain boundaries” in the MXene film and increasing flake size enhances electrical conductivity⁴⁰. Therefore, optimizing the flake size in the case of lift-off-based patterning poses a trade-off between improving electrical conductivity or patterning lateral resolution which will be better with larger and smaller flakes, respectively.

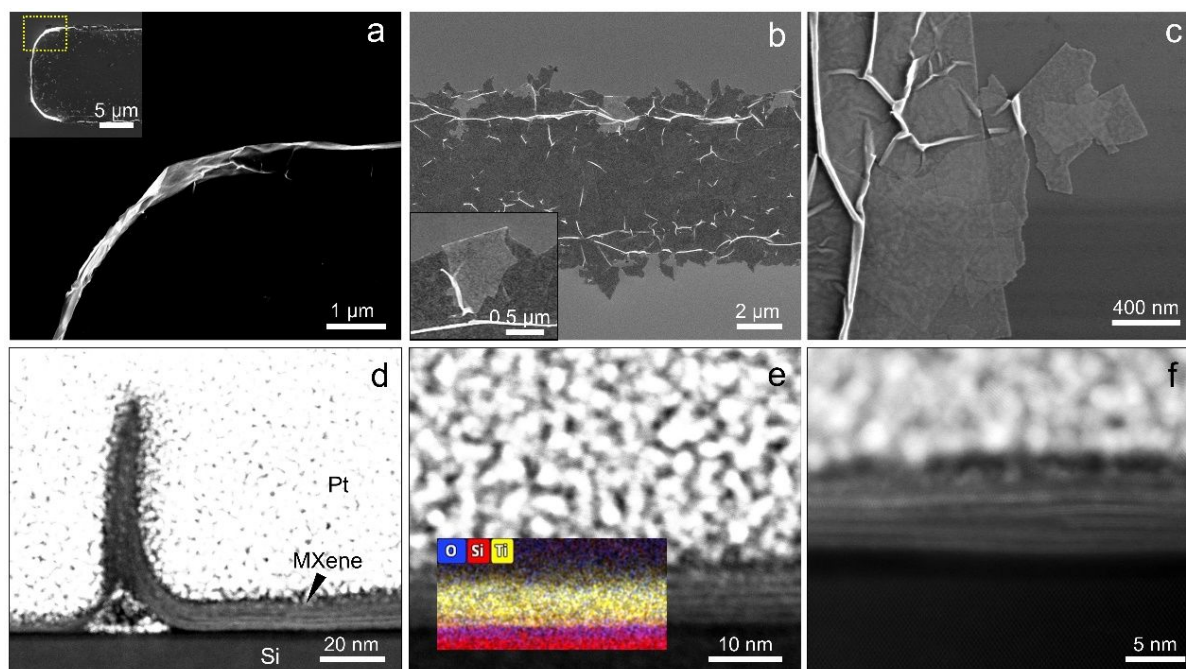
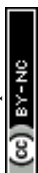


Fig. 2 MXene thin-film pattern imperfections. (a) SEM image of vertical MXene flakes at outlining the edge of a 15 μm electrode, the whole edge area is shown at lower magnification in the insert. (b) SEM image of a 5 μm electrode demonstrating spill outs and back folding of flakes, insert shows a zoom-in on a back-folded flake. (c) High-resolution SEM image showing the folds of relatively large wrinkles, small homogenous ripples in the MXene flakes, and spill-out of a few flakes at a pattern edge. (d) STEM images of the MXene thin-film cross section showcasing (d) a typical large wrinkle fold at the edge of a pattern, (e) typical section overlaid with EDS mapping of O (blue), Si (red) and Ti (yellow), and (f) high-resolution image of MXene line defect formed at flake intersections.

AFM measurements were used to analyze the thin-film thickness distribution, indicating an average thickness 3-5 MXene layers (Fig. 3a). The number of layers corresponds with the thickness observed for a single layer ~1.5 nm (Fig. 3c), which agrees with the d-spacing of a free-standing film determined by XRD (Fig. 2d). This specific thickness depends on the termination groups, remaining intercalated lithium ions, and water molecules – factors governed by the synthesis method⁴². The average deposited MXene thin-film thickness is



about ~ 6 nm (Fig. 3b). Further AFM measurements confirm the deposition uniformity by sampling a very large area of over $\geq 1000 \mu\text{m}^2$ in total (Fig. S11). The AFM scans in high vertical resolution confirm the complete removal of the 3D halide salt residues. For the patterned electrodes the thickness in the uniform areas was found to be either ~ 6 or ~ 7.5 nm on average (corresponding to 4 or 5 flakes) (Fig. S11 and S12). This is also corroborated by TEM analysis of the cross-section (Fig. S13). Near the edges of the electrodes there is some localized increase in thickness up to ~ 20 - 40 nm (Fig. 3g,h) and evens out over the span of about 5 to 10 μm (Fig. S12). Increased thickness at electrode edges following lift-off is expected¹⁸. This increased thickness arises from the wrinkles and folds created in MXene flakes upon removal of the photoresist walls as discussed above. This may pose some limitations to the width of thin-film MXene features with thickness below 10 nm produced using this method.

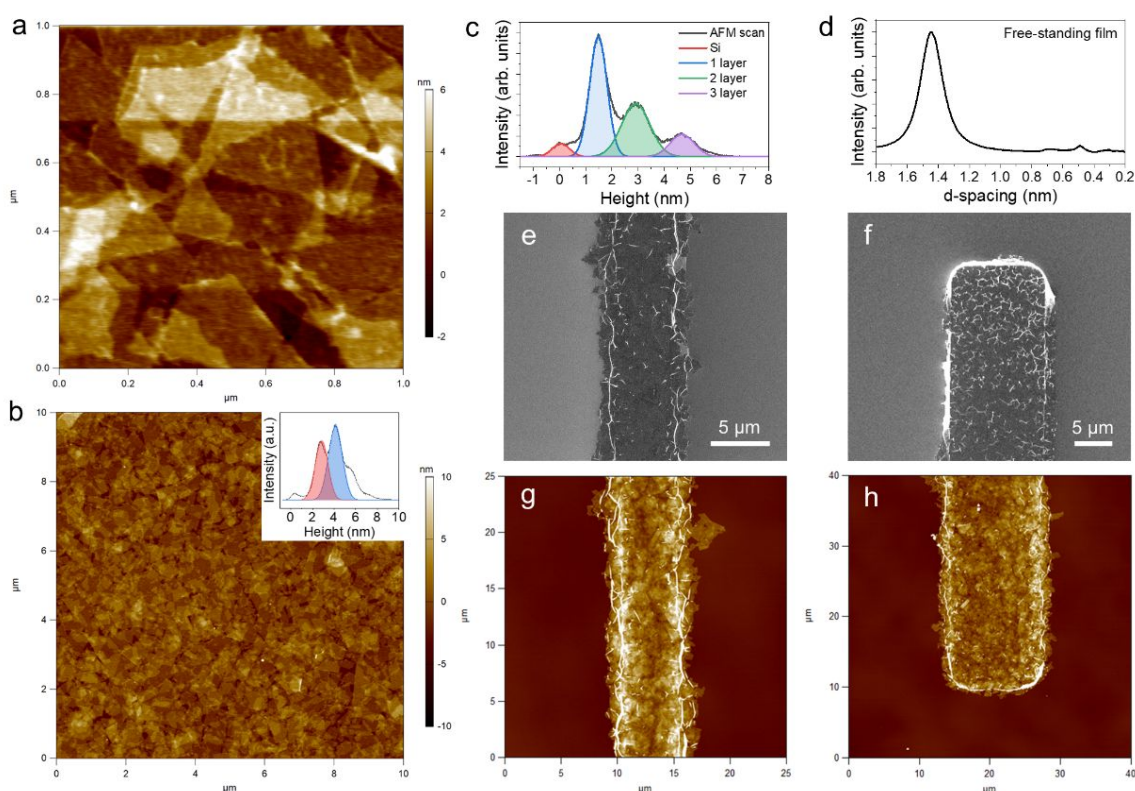


Fig. 3 Analysis of spin-coated MXene thin films thickness. AFM measurements of MXene coating of (a) 1×1 and (b) $10 \times 10 \mu\text{m}^2$ scan area, (b) inset shows a histogram of the thickness with the red and blue fits corresponding to 2 and 3 MXene flakes, respectively. (c) Histogram of the thickness of scan (a) with the green, red, and blue fits corresponding to 1, 2, and 3 flakes. (d) XRD spectrum as a function of d-spacing for a free-standing MXene film made from the coating solution. SEM images of patterned MXene electrodes with a width of (e) 5 and (f) 15 μm , and corresponding AFM scans of the (g) 5 and (h) 15 μm wide electrodes, that share the same color bar scale.

3.4 Optical and electrical properties

Spin-coating of a ~ 6 nm thin film of MXene is demonstrated on sapphire and glass dies (Fig. 4). The sheet resistance of the MXene coated sapphire was measured at $770 \Omega/\text{sq}$ (Fig. 4c), corresponding to a conductivity of 2164 S/cm . The electrical resistance of MXene films depends on multiple factors: the film thickness, MXene stoichiometry, flakes defects, film



packing density, and flake size⁴⁰. The sheet resistance could be increased by enlarging the flake size²¹ but doing so will impact the resolution limit of the deposition after photolithography.

To measure the transparency and repeatability of the MXene coatings, glass substrates were coated in single and multiple spin-coating cycles (Fig. 4d). $\text{Ti}_3\text{C}_2\text{T}_z$ MXene absorbs about ~3 % of visible light for a single MXene layer^{16,43}. After one spin-coating cycle the film absorbs approximately 11.5 % at 550 nm, and each additional cycle consistently absorbs another ~10 % (Fig. 4d insert), following the expected linear relation of Beer–Lambert law. The absorbance band at around ~800 nm is related to the surface plasmon of $\text{Ti}_3\text{C}_2\text{T}_z$ and the decrease above ~1400 nm is also typical behavior of this material²⁹. The measured transparency and sheet resistance of the spin-coated films agree with values measured for $\text{Ti}_3\text{C}_2\text{T}_z$ MXene thin films of similar thickness²¹. Overall, the single-cycle spin-coated films exhibit sufficiently high transparency (~88.5 % at 550 nm) and high conductivity (>2000 S/cm) for transparent electronic applications¹⁷.

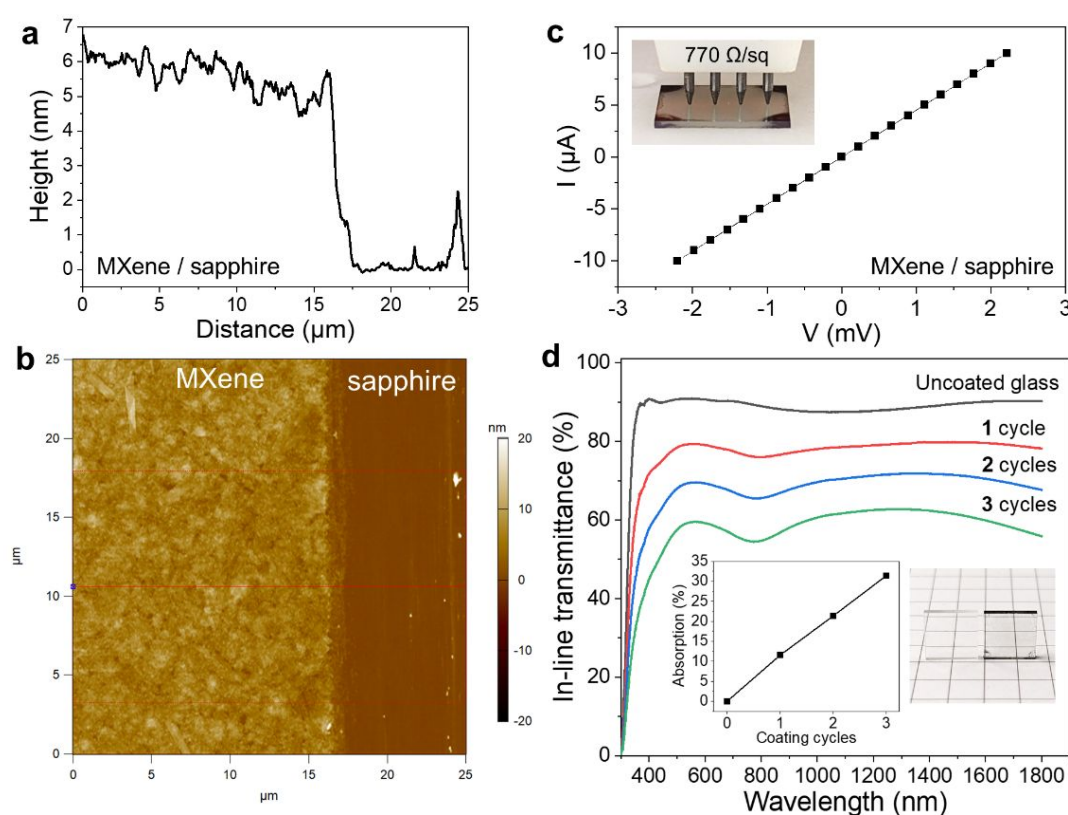


Fig. 4 Transparent uniform spin-coated $\text{Ti}_3\text{C}_2\text{T}_z$ MXene film on sapphire and glass. (a) average height of the film corresponding to the area marked in (b), and the matching AFM scan. (c) I-V curve of MXene coated sapphire and a photograph of the sample and 4-point probe setup. (d) In-line transmittance of MXene coating on glass for up to three spin coating cycles. Inserts show the absorbance values at 550 nm and a photograph of uncoated and spin-coated glass after a single cycle.

The electrical properties of the fabricated electrodes and the MXene–Si junction were probed to assess the performance of the patterned thin films (Fig. 5). The resistance of 50 and 100 μm wide MXene electrodes was 3251 and 1372 Ω , respectively (Fig. 5a). The estimated conductivities based on the approximate electrodes cross-sections (measured by AFM) are ~1350 and ~2200 S/cm for a width of 50 and 100 μm , respectively. These values are in good agreement with the conductivity of MXene thin films measured by others⁴⁴.



$\text{Ti}_3\text{C}_2\text{T}_z$ is a metallic conductor with a work function ranging from 3.9 to 4.8 eV, depending on the termination groups¹⁴. Using XPS⁴⁵ the work function of our MXene was determined to be 4.19 eV (Fig. S1d). Due to the selection of the n-type Si and the MXene work function, the MXene patterns on Si wafer create Van der Waals Schottky diodes. The diode I-V characteristics depend on the electrode dimensions which determine the MXene–Si contact area (Fig. 5b). The MXene thin film is transparent to visible light and upon increasing the illumination luminous flux from 0.08 to 1.38 mW/cm² increased the recombination current by three orders of magnitude (Fig. 5c). MXene–Si–MXene acts as a 2-terminal planar structure metal–semiconductor–metal (MSM) photodetector. The MSM junction I-V characteristic under different illumination intensities exhibits high sensitivity to light under relatively low photon flux (0.08–1.38 mW/cm²) (Fig. 5d,e). Although similar observations have been made previously by Kang et al.⁴⁶, it was demonstrated under two orders of magnitude higher flux (40–106 mW/cm²). The MXene–Si Schottky diode exhibits a low reverse current of 28 nA at -100 V (Fig. 5f). The I-V characteristics of the diode were not affected after scanning from -100 to 50 V. A zoom-in view illustrates the recombination current barrier region (Fig. 5f). Typically, making photodetectors requires utilizing transparent semiconductors like indium tin oxide (ITO) and ruthenium oxide (RuO) without employing complex fabrication methods involving backside illumination³². Alternatively, our method allows fabrication of complex architecture transparent diodes by simple MXene micropatterning at room temperature without any high vacuum deposition. We show that the patterned film thickness and line dimensions can be reduced to several nanometers and $\leq 100 \mu\text{m}$, respectively, without dramatically hindering the MXene performance. The resistance of the MXene remains negligible compared to the MXene–Si–MXene junction, enabling to easily create transparent MXene electrodes for sensitive photodetectors^{47,48}.

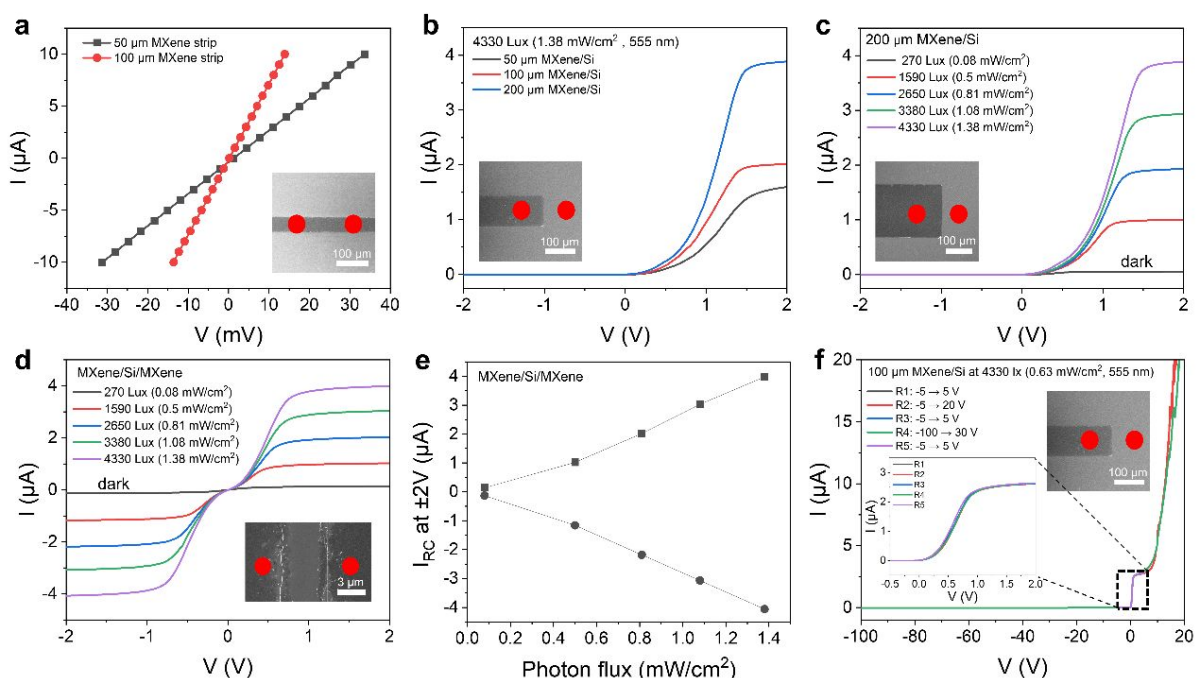
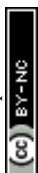


Fig. 5 Electrical properties of MXene patterned electrodes on Si. (a) Four-point probe I-V measurements of 50 and 100 μm wide electrodes. The insert shows an SEM image of the probed region, and the red dots mark the approximate placement of the probes. (b) I-V measurements of 50, 100, and 200 μm electrodes serving as Schottky diodes. (c) 200 μm MXene diode under different illumination intensities. (d) Voltage measurements across a



MXene–Si–MXene junction under different light intensities. (e) Recombination current as a function of photon flux for the measurement shown in (d). (f) 100 μm -wide MXene diode I-V curve before and after operation at relatively high voltages (-100 – 50 V). Insert shows a zoom-in view of the indicated recombination current region.

View Article Online
DOI: 10.1039/D4NA00983E

4. Conclusions

Spin coating is a standard nanofabrication technique that can be employed for deposition of MXene thin films using colloidal solutions. However, the presence of halide salt residues can cause problems during ensuing fabrication processes or device operation. Herein, we present a straightforward approach for controlled deposition and patterning of extremely thin (<10 nm) and halide-residue free 2D MXene features at ambient conditions. The process involves three steps: (1) spin coating for MXene deposition, (2) cleaning halide salt residues by HCl spin-cleaning, and (3) lift-off of a developed photoresist to achieve desired patterns with a lateral resolution of ~ 1.5 μm . The deposition process is repeatable and can be done consecutively to achieve targeted film thickness. The patterned MXene was thoroughly characterized by high resolution electron microscopy and AFM. The transparent electrodes exhibited conductivities of approximately 1300 and 2200 S/m, for a width of 100 and 50 μm , respectively. The MXene–Si Schottky diode characteristics were assessed and displayed high sensitivity to light under a photon flux of 0.08–1.38 mW/cm^2 . The combination of spin-coating followed by HCl spin-cleaning to eliminate salt residues offers significant advantages, addressing one of the main drawbacks associated with deposition of MXene films.

Acknowledgements

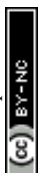
This work was supported by the Israel Science Foundation (grant No. 2527/22).

Conflicts of interest

The authors declare there are no conflicts to declare.

References

- Morris, P. R. A History of the World Semiconductor Industry. *A History of the World Semiconductor Industry* (1990) doi:10.1049/PBHT012E.
- Wang, H., Yao, Z., Acauan, L., Kong, J. & Wardle, B. L. Toward MXene interconnects. *Matter* **4**, 1447–1449 (2021).
- Lin, Z., Huang, Y. & Duan, X. Van der Waals thin-film electronics. *Nature Electronics* **2019** 2:9 **2**, 378–388 (2019).
- Kim, J. H. *et al.* Centimeter-scale Green Integration of Layer-by-Layer 2D TMD vdW Heterostructures on Arbitrary Substrates by Water-Assisted Layer Transfer. *Scientific Reports* **2019** 9:1 **9**, 1–10 (2019).
- Kumar, R., Kumari, B., Kumar, S., Sahoo, M. & Sharma, R. Temperature and Dielectric Surface Roughness dependent Performance Analysis of Cu-Graphene Hybrid Interconnects. *IEEE Electrical Design of Advanced Packaging and Systems Symposium 2020-December*, (2020).
- Chen, X. *et al.* Fully integrated graphene and carbon nanotube interconnects for gigahertz high-speed CMOS electronics. *IEEE Trans Electron Devices* **57**, 3137–3143 (2010).



7. Liang, X. *et al.* Toward clean and crackless transfer of graphene. *ACS Nano* **5**, 9144–9153 (2011). View Article Online
DOI: 10.1039/D4NA00983E
8. Gogotsi, Y. & Anasori, B. The Rise of MXenes. *ACS Nano* **13**, 8491–8494 (2019).
9. Anasori, B. & Gogotsi, Y. 2D Metal carbides and nitrides (MXenes): Structure, properties and applications. *2D Metal Carbides and Nitrides (MXenes): Structure, Properties and Applications* 1–534 (2019) doi:10.1007/978-3-030-19026-2/COVER.
10. The pull of the MXene vortex. *Nat Nanotechnol* **17**, 1025 (2022).
11. Lim, K. R. G. *et al.* Fundamentals of MXene synthesis. *Nature Synthesis* **2022 1:8 1**, 601–614 (2022).
12. Shuck, C. E. *et al.* Scalable Synthesis of Ti₃C₂T_x MXene. *Adv Eng Mater* **22**, 1901241 (2020).
13. Moon, J. H. *et al.* Materials Quest for Advanced Interconnect Metallization in Integrated Circuits. *Advanced Science* **10**, 2207321 (2023).
14. Schultz, T. *et al.* Surface Termination Dependent Work Function and Electronic Properties of Ti₃C₂T_x MXene. *Chemistry of Materials* **31**, 6590–6597 (2019).
15. Hart, J. L. *et al.* Control of MXenes' electronic properties through termination and intercalation. *Nature Communications* **2019 10:1 10**, 1–10 (2019).
16. Yun, T. *et al.* Electromagnetic Shielding of Monolayer MXene Assemblies. *Advanced Materials* **32**, 1906769 (2020).
17. Hantanasirisakul, K. *et al.* Fabrication of Ti₃C₂T_x MXene Transparent Thin Films with Tunable Optoelectronic Properties. *Adv Electron Mater* **2**, 1600050 (2016).
18. Xu, X., Guo, T., Lanza, M. & Alshareef, H. N. Status and prospects of MXene-based nanoelectronic devices. *Matter* **6**, 800–837 (2023).
19. Wang, Z., Kim, H. & Alshareef, H. N. Oxide Thin-Film Electronics using All-MXene Electrical Contacts. *Advanced Materials* **30**, 1706656 (2018).
20. Mojtabavi, M. *et al.* Wafer-Scale Lateral Self-Assembly of Mosaic Ti₃C₂T_xMXene Monolayer Films. *ACS Nano* **15**, 625–636 (2021).
21. Guo, T. *et al.* Rational Design of Ti₃C₂T_x MXene Inks for Conductive, Transparent Films. *ACS Nano* **17**, 3737–3749 (2023).
22. Zhang, C. (John) *et al.* Additive-free MXene inks and direct printing of micro-supercapacitors. *Nature Communications* **2019 10:1 10**, 1–9 (2019).
23. Mariano, M. *et al.* Solution-processed titanium carbide MXene films examined as highly transparent conductors. *Nanoscale* **8**, 16371–16378 (2016).
24. Xu, X. *et al.* High-Yield Ti₃C₂T_x MXene–MoS₂ Integrated Circuits. *Advanced Materials* **34**, 2107370 (2022).
25. Montazeri, K. *et al.* Beyond Gold: Spin-Coated Ti₃C₂-Based MXene Photodetectors. *Advanced Materials* **31**, 1903271 (2019).



26. Jiang, Q. *et al.* On-Chip MXene Microsupercapacitors for AC-Line Filtering Applications. *Adv Energy Mater* **9**, 1901061 (2019). View Article Online
DOI: 10.1039/D4NA00983E
27. Kim, E. *et al.* Scalable fabrication of MXene-based flexible micro-supercapacitor with outstanding volumetric capacitance. *Chemical Engineering Journal* **450**, 138456 (2022).
28. Xu, B. *et al.* Ultrathin MXene-Micropattern-Based Field-Effect Transistor for Probing Neural Activity. *Advanced Materials* **28**, 3333–3339 (2016).
29. Hazan, A. *et al.* MXene-Nanoflakes-Enabled All-Optical Nonlinear Activation Function for On-Chip Photonic Deep Neural Networks. *Advanced Materials* **35**, 2210216 (2023).
30. Ahn, S. *et al.* A 2D Titanium Carbide MXene Flexible Electrode for High-Efficiency Light-Emitting Diodes. *Advanced Materials* **32**, 2000919 (2020).
31. Reinhardt, K. A. & Kern, W. Handbook of Silicon Wafer Cleaning Technology, Third Edition. *Handbook of Silicon Wafer Cleaning Technology, Third Edition* 1–773 (2018)
doi:10.1016/C2016-0-01001-X.
32. Luo, L. *et al.* MXene-GaN van der Waals metal-semiconductor junctions for high performance multiple quantum well photodetectors. *Light: Science & Applications* **2021 10:1** **10**, 1–11 (2021).
33. Li, G. *et al.* Terahertz Polarizers Based on 2D Ti₃C₂T_z MXene: Spin Cast from Aqueous Suspensions. *Adv Photonics Res* **1**, 2000084 (2020).
34. Li, B. *et al.* Patterning of Wafer-Scale MXene Films for High-Performance Image Sensor Arrays. *Advanced Materials* **34**, 2201298 (2022).
35. Lee, D. *et al.* Centrifugal-Gravity-Enforced Deposition of MXene Electrodes for High-Performance and Ultrastable Microsupercapacitors. *ACS Appl Mater Interfaces* **16**, 26004–26014 (2024).
36. Michael, P. R., Johnston, D. E. & Moreno, W. A. Calculation of Irradiance from Illuminance for Artificial Light Photovoltaics Applications. *IEEE Instrum Meas Mag* **26**, 52–58 (2023).
37. Natu, V., Sokol, M., Verger, L. & Barsoum, M. W. Effect of Edge Charges on Stability and Aggregation of Ti₃C₂T_z MXene Colloidal Suspensions. *Journal of Physical Chemistry C* **122**, 27745–27753 (2018).
38. Song, O. *et al.* All inkjet-printed electronics based on electrochemically exfoliated two-dimensional metal, semiconductor, and dielectric. *npj 2D Materials and Applications* **2022 6:1** **6**, 1–12 (2022).
39. Sarycheva, A., Shanmugasundaram, M., Krayev, A. & Gogotsi, Y. Tip-Enhanced Raman Scattering Imaging of Single- to Few-Layer Ti₃C₂T_xMXene. *ACS Nano* **16**, 6858–6865 (2022).
40. Zhang, J. *et al.* Scalable Manufacturing of Free-Standing, Strong Ti₃C₂T_x MXene Films with Outstanding Conductivity. *Advanced Materials* **32**, 2001093 (2020).
41. Song, T. E. *et al.* Vertically Aligned Nanopatterns of Amine-Functionalized Ti₃C₂ MXene via Soft Lithography. *Adv Mater Interfaces* **7**, 2000424 (2020).



42. Natu, V. *et al.* Effect of Base/Nucleophile Treatment on Interlayer Ion Intercalation, Surface Terminations, and Osmotic Swelling of Ti₃C₂TzMXene Multilayers. *Chemistry of Materials* **34**, 678–693 (2022). [View Article Online](#)
DOI: 10.1039/D4NA00983E
43. Dillon, A. D. *et al.* Highly Conductive Optical Quality Solution-Processed Films of 2D Titanium Carbide. *Adv Funct Mater* **26**, 4162–4168 (2016).
44. Lipatov, A. *et al.* Effect of Synthesis on Quality, Electronic Properties and Environmental Stability of Individual Monolayer Ti₃C₂ MXene Flakes. *Adv Electron Mater* **2**, 1600255 (2016).
45. Whitten, J. E. Ultraviolet photoelectron spectroscopy: Practical aspects and best practices. *Applied Surface Science Advances* **13**, 100384 (2023).
46. Kang, Z. *et al.* MXene–Silicon Van Der Waals Heterostructures for High-Speed Self-Driven Photodetectors. *Adv Electron Mater* **3**, 1700165 (2017).
47. Koppens, F. H. L. *et al.* Photodetectors based on graphene, other two-dimensional materials and hybrid systems. *Nature Nanotechnology* **2014 9:10 9**, 780–793 (2014).
48. Li, L. & Shen, G. MXene based flexible photodetectors: progress, challenges, and opportunities. *Mater Horiz* **10**, 5457–5473 (2023).



Data Availability Statement

View Article Online
DOI: 10.1039/D4NA00983E

The data supporting the findings of this study are available from the corresponding author upon reasonable request. Specific datasets, including experimental protocols, characterization data, and analysis results, can be provided to researchers with legitimate interests in replicating or expanding upon this work.

